CellPress
OPEN ACCESS

One Earth

Article

An updated global mercury budget from a coupled atmosphere-land-ocean model: 40% more re-emissions buffer the effect of primary emission reductions

Yanxu Zhang,[1,2,9,*] Peng Zhang,[1] Zhengcheng Song,[1] Shaojian Huang,[1] Tengfei Yuan,[1] Peipei Wu,[1] Viral Shah,[3] Maodian Liu,[4] Long Chen,[5] Xuejun Wang,[6] Jun Zhou,[7] and Yannick Agnan[8]

[1]School of Atmospheric Sciences, Nanjing University, Nanjing, Jiangsu, China
[2]Frontiers Science Center for Critical Earth Material Cycling, Nanjing University, Nanjing, Jiangsu, China
[3]Harvard John A. Paulson School of Engineering and Applied Sciences, Harvard University, Cambridge, MA, USA
[4]School of the Environment, Yale University, New Haven, CT, USA
[5]Key Laboratory of Geographic Information Science (Ministry of Education), School of Geographic Sciences, East China Normal University, Shanghai, China
[6]Ministry of Education Laboratory of Earth Surface Processes, College of Urban and Environmental Sciences, Peking University, Beijing, China
[7]Department of Environmental, Earth, and Atmospheric Sciences, University of Massachusetts Lowell, Lowell, MA, USA
[8]Earth and Life Institute, Université Catholique de Louvain, 1348 Louvain-la-Neuve, Belgium
[9]Lead contact
*Correspondence: zhangyx@nju.edu.cn
https://doi.org/10.1016/j.oneear.2023.02.004

SCIENCE FOR SOCIETY Mercury is a toxic metal that mainly affects human health through seafood consumption. The Minamata Convention on Mercury, an international agreement, aims to protect human health by reducing mercury emissions. However, the mercury in our environment is not only from current anthropogenic sources but also from re-emissions from land and ocean that have accumulated historical emissions. To effectively reduce environmental mercury levels, it is crucial to have a complete understanding of the global mercury budget.

In our study, we integrated the latest advances in atmospheric mercury redox chemistry, vegetation uptake, seawater sources, and riverine discharges through use of a coupled air-land-sea model. Our findings indicate 40% higher total mercury emission than previously estimated, mainly because of higher ocean re-emissions. This highlights the need for more aggressive emission reduction efforts to achieve the goal set by the Minamata Convention on Mercury.

SUMMARY

The effectiveness of reducing the environmental level of mercury (Hg) by controlling anthropogenic emissions depends on the magnitude of re-emissions from the land and ocean, which requires a comprehensive understanding of its global biogeochemical cycle. Recent advances in atmospheric Hg redox chemistry, vegetation uptake, seawater Hg sources, and riverine discharges greatly challenge our understanding of the global Hg cycle, but the overall effects remain understudied. Here, we develop a new coupled atmosphere-land-ocean model and find potentially 40% higher total atmospheric Hg emissions than previously recognized primarily because of higher re-emissions from the ocean. Our results suggest a likely smaller sensitivity of environmental Hg levels to anthropogenic emission changes, stressing that potentially more aggressive emission control is required to decrease Hg levels.

INTRODUCTION

Mercury (Hg) and its compounds are neurotoxic and cause significant health impacts on the global population.[1] The Hg in the environment is from anthropogenic (e.g., coal burning in power plants and gold mining) and natural (e.g., volcanic eruption and hydrothermal vents) sources.[2] Hg from these sources can be deposited into the land/ocean and partially re-emitted into the atmosphere; these emissions are at least 2- to 3-fold larger than the primary emissions.[3] The Minamata Convention on Mercury, an

international legally binding treaty that aims to reduce the anthropogenic emissions and health impacts caused by Hg, is in effect since 2017 (https://www.mercuryconvention.org). However, the effectiveness of the convention largely depends on the magnitude of the re-emissions and requires a comprehensive understanding of the global Hg cycle.

By synthesizing our understanding of Hg biogeochemistry and measurements in different environmental compartments, previous studies have developed several global budgets of Hg cycling.[3–8] These budgets generally agree that the present-day total atmospheric emissions are ~9,000 Mg year^{-1} with anthropogenic emissions of ~2,000 Mg year^{-1} and land and ocean re-emissions contributing ~2,000 and ~5,000 Mg year^{-1}, respectively. The atmospheric deposition is balanced to the total emissions, with land and ocean receiving ~3,000 and ~6,000 Mg year^{-1}, respectively, making a net burial of anthropogenic emissions to land and ocean ~1,000 Mg year^{-1} each. Divalent Hg (Hg^{II}) is the dominant form of deposition, contributing approximately two-thirds of the total flux to the land and ocean, with the remaining in the form of elemental Hg (Hg^0). Geogenic emissions and burial of Hg at the deep ocean floor are generally much less (~300 Mg year^{-1}).

Such a budget is challenged by recent advances in our understanding of the global Hg cycle: (1) updated atmospheric Hg redox chemistry that considers the photo-reduction of Hg^{II} species,[9,10] (2) atmospheric Hg^0 uptake by leaf stomata is found to be the dominant source of Hg in terrestrial ecosystems such as tundra and Amazon forests,[11,12] (3) seawater Hg isotope data suggest that the atmospheric deposition of Hg^0 and Hg^{II} contributes approximately equally to the ocean,[13] and (4) a new spatial estimate suggested that global riverine Hg export has been underestimated by many previous studies.[14] The implications of these findings for the global Hg cycle, especially their interactions, are expected to be important but remain understudied.

In this study, we synthesize these new findings and develop an updated global Hg budget. We use a coupled atmosphere-land-ocean model system to incorporate these updates in multiple environmental compartments (see Experimental procedures for details). The model system consists of the GEOS-Chem (https://www.geos-chem.org; version 12.9.0),[10] global terrestrial mercury model (GTMM),[5] and MITgcm[15] models for the atmosphere, land, and ocean, respectively, coupled dynamically by the NJUCPL coupler.[16] The model results are evaluated against the reference models (i.e., the original GEOS-Chem, GTMM, and MITgcm model version without our modifications) and available measurement data. Our findings indicate that the land is a more significant sink for atmospheric Hg and that the ocean may be a larger source of re-emission than previously estimated by modeling studies. Our model also reveals a 40% increase in total atmospheric Hg emissions and a shorter atmospheric residence time. This suggests that reducing environmental Hg levels, as required by the Minamata Convention on Mercury, may require more stringent emission control measures because the environment may be less sensitive to changes in anthropogenic emissions in the future.

RESULTS AND DISCUSSION

Updated Hg budget

Figure 1 shows the updated budget for the global Hg cycle, simulated by the coupled atmosphere-land-ocean model using the reference year of 2012. The primary atmospheric emissions are from anthropogenic sources (2,340 Mg year^{-1})[17] and volcanoes (250 Mg year^{-1}).[10] The model agrees with observed near-ground atmospheric Hg concentrations and wet deposition fluxes, mainly in North America, western Europe, and East Asia (Figures S1 and S2). The simulated Hg^{II} deposition to land (including particulate bound Hg^{II} [Hg(P)], the same after therein) is estimated as 1,870 Mg year^{-1} (dry: 960 Mg year^{-1}; wet: 910 Mg year^{-1}), consistent with previous modeling studies (e.g., 1,600 Mg year^{-1}).[10] We simulate a twice-higher global Hg^0 dry deposition to land (gross flux of 2,220 Mg year^{-1}; i.e., not counting land re-emissions, same in hereafter except noted) than previous models (e.g., 1,200 Mg year^{-1}),[10] reflecting higher vegetation stomatal uptake as a result of higher biological reactivity of Hg^0 mainly over tropical/subtropical forests such as the Amazon and Southeast Asia[18] (Figure S3). This is consistent with most recent field studies and syntheses,[19,20] which estimate global flux ranging from 2,110–3,810 Mg year^{-1}. The spatial pattern also agrees with data-derived soil Hg concentrations in the topsoil.[21]

Direct measurement data of terrestrial Hg^0 re-emissions remain sparse. Agnan et al.[22] developed an observational data-derived estimate of global terrestrial Hg re-emissions. They synthesized available chamber- and micrometeorological-derived flux data measured at land-air interfaces and estimated global total land Hg^0 re-emissions from −513 to 1,353 Mg year^{-1} as a 25% confidential interval (Figure S3). Although they reported their estimates as net fluxes (i.e., gross Hg^0 re-emission – gross Hg^0 deposition), these fluxes are close to the gross Hg^0 re-emissions because most of the data available are soil-air exchange fluxes under the canopy and do not consider the foliar intake that is the major pathway for Hg^0 deposition to land.[20,22] The GTMM adopted in this study is the first mechanistic model for soil inorganic Hg storage and re-emissions considering the vegetation uptake and soil organic carbon pools,[5] but it generally simulates too-high soil re-emissions (2,900 Mg year^{-1}), which is close to the total atmospheric deposition flux to land (3,260 Mg year^{-1}) used to drive the GTMM model. This is much higher than the estimate by Agnan et al.[22] and may not be consistent with the accumulation of a large mass of Hg in the terrestrial environment.[23] This overestimation may be caused by (1) a high photoreduction rate of Hg^{II} deposition in the surface soil/leaf pool, (2) a low fraction of deposited Hg^0 associated with stomata, and (3) a high fraction of Hg^0 re-emission from soil organic pools.[24] By adjusting these parameters (Experimental procedures), the simulated Hg^0 re-emissions from the global land (including soils and vegetation) in this study are reduced to 1,330 Mg year^{-1} (Figure 1), which is slightly higher than in previous studies (e.g., 1,100 Mg year^{-1})[4,10] that derived the land re-emissions by mass balance with global atmospheric depositions. Our results are more consistent with recent findings of greater retention of Hg in the terrestrial environment[19,25] and the estimate by Agnan et al.[22]

Observations of Hg^0 and Hg^{II} deposition fluxes remain sparse over the ocean, but the ratio diagnosed by isotopic signature is a more reliable constraint. A recent study uses marine even-MIF (mass-independent fractionation; $\Delta^{200}Hg$) composition measurements and suggests a ratio of 1:1.[13] The ratio is much higher than those from previous modeling studies that suggest a ratio of

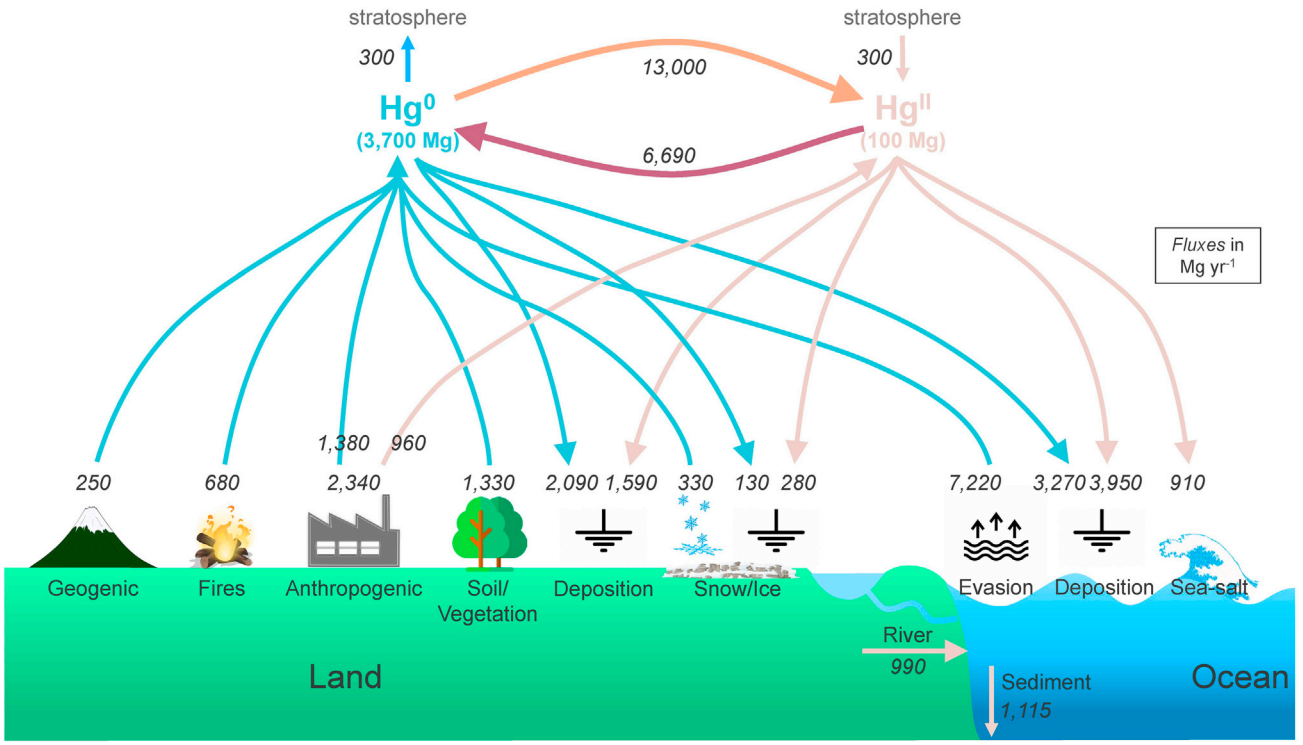

Figure 1. Updated global atmospheric Hg budget at present day (the reference year 2012)

Blue and brown arrows are for Hg^0 and Hg^{II}, respectively. Masses of Hg in the troposphere have a unit of megagrams and all fluxes (in italics) have a unit of megagrams per year. Hg^{II}-related fluxes and masses also include Hg(P). The fluxes from/to land constitute the total of soil and vegetation. The Hg^{II} deposition flux to the ocean is separated into two terms: dry/wet deposition and uptake by sea salt. All fluxes are gross ones, and the net fluxes can be calculated by differencing two competing gross fluxes.

1:2.0[10] or 1:2.7.[26] We speculate that previous models may have underestimated Hg^0 dry deposition to the ocean (or air-sea exchange). The exchange velocity (k) depends on wind speed (u) with different parameterizations derived from *in situ* measurements of CO_2, O_2, or dimethyl sulfide (DMS), as summarized by Zhang et al.[16] and Osterwalder et al.[27] These parameterizations use a linear, quadratic, or cubic form of wind speed,[28–33] and a quadratic form has been widely used in past Hg modeling studies analogous to CO_2.[6,10,16,26] However, the different parameterizations in the literature indicate additional driving factors, such as wave breaking and bubble formation, which are dependent on the properties of different gases, and no single wind speed parameterization exists for all gases.[34] Indeed, the first direct measurement of Hg^0 air-sea exchange flux using micrometeorological methods suggests a cubic form of wind function, reflecting the stronger influence of wave and bubble conditions on lower-solubility gases such as Hg^0 (45 μg L^{-1} at 20°C versus 9.1 mg L^{-1} for O_2 and 1.7 g L^{-1} for CO_2).[27] However, direct application of this function ($k = 0.18\,u^3$) to the global ocean may not be feasible because it only represents the shallow coastal conditions of the Baltic Sea, the dynamic range of wind speed is relatively narrow, and the variability of the measurements is still high.[27]

We thus adopt the McGillis et al.[31] scheme, which has been tested in global models.[16] This scheme also uses a cubic function of wind speed but with a smaller pre-cubic term coefficient ($k = 3.3 + 0.026\,u^3$). The resulting global deposition of Hg^0 and Hg^{II} to the ocean is simulated as 3,270 Mg $year^{-1}$ and 4,860 Mg $year^{-1}$ (including a dry deposition flux of 910 Mg $year^{-1}$ via uptake by sea salt), respectively, with a Hg^0:Hg^{II} ratio of 1:1.5 (Figure 1), more consistent with the marine isotope-derived constraint. It also results in a gross ocean emission of 7,220 Mg $year^{-1}$ and a net Hg^0 evasion flux (i.e., gross emission – gross deposition) of 3,950 Mg $year^{-1}$, which is higher than previous estimates (e.g., 3,360 Mg $year^{-1}$ by Zhang et al.[16] and 2,900 Mg $year^{-1}$ by Horowitz et al.[26]) but is still within the constraint of available observations (Figures S4 and S5). The modeled increase in net Hg^0 evasion also enhances the atmospheric Hg pool in the marine boundary layer, which thus increases the atmospheric deposition to the ocean. An alternative hypothesis to get a higher Hg^0:Hg^{II} ratio is a lower Hg^{II} deposition flux.[13] However, observational evidence for this hypothesis is lacking so far. We thus suggest that it has a lower possibility than a higher Hg^0 flux because of our better understanding of the Hg^{II} deposition process than Hg^0.[35] Lower Hg^{II} deposition flux over the ocean may also mean an equivalent lower flux over land, which is generally not supported by land-based Hg^{II} wet deposition observations (Figure S1).

In our new model, the previous estimate of riverine Hg discharge to the global ocean (5,400 Mg $year^{-1}$)[24] was substituted for a five-times lower estimate (1,000 Mg $year^{-1}$).[14] The impact of riverine export on the global Hg cycle seems small at a decadal timescale, probably associated with the refractory nature of the riverine particulate Hg^{II}, with more than 80%

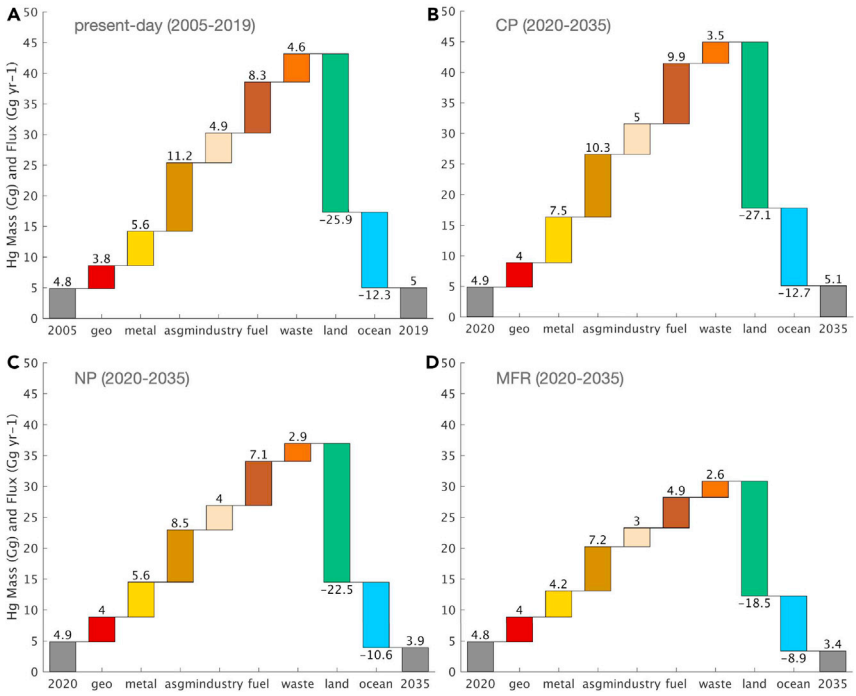

Figure 2. Cumulate primary atmospheric Hg emission sources and their sinks

(A–D) 2005–2019 (A) and 2020–2035 (B–D) for three future emission scenarios: (B) Current policy (CP), (C) new policy (NP), and (D) maximum feasible reduction (MFR). Emission sectors include geogenic (geo), metal production (metal), artisanal and small-scale gold mining (asgm), industry, fossil fuel combustion (fuel), and waste incineration (waste). 1 Gg = 10^3 Mg.

deposited in the coastal environment[14,36] (Figure S6). However, the impact of riverine discharge on the coastal environment could be significant (Figures S6 and S7).[37] Coastal oceans are the most biologically productive parts of the entire ocean, and a substantial fraction of fish and shellfish consumed by the world population is from near-shore aquaculture and capture.[38] Indeed, Hg accumulation flux one to two orders of magnitude higher over coastal regions than the open ocean is simulated by the model, consistent with observations (Figures S5 and S8). Additionally, we noticed that these regions could be a net source of Hg to the atmosphere as a result of the riverine discharge; i.e., the net evasion of Hg^0 surpasses the atmospheric deposition of Hg^{II}[39] (Figures S9–11).

The model suggests that 1,670 Mg $year^{-1}$ of Hg from direct anthropogenic emissions are sequestered in the global land and 910 Mg $year^{-1}$ in the global ocean. This reflects a potential regimen shift in our understanding of the fate of primary atmospheric emissions: from mainly sequestered in the ocean to the land. Selin et al.[4] developed a preindustrial Hg budget with soil and ocean sequestering 40 Mg $year^{-1}$ and 460 Mg $year^{-1}$ of the geogenic emissions, respectively. Horowitz et al.[26] simulated a present-day sink of 780 Mg $year^{-1}$ and 1,700 Mg $year^{-1}$ by land and ocean, respectively. The updated atmospheric Hg redox chemistry simulates more Hg^{II} deposition to the land with a net sink of 1,400 Mg $year^{-1}$ and 1,100 Mg $year^{-1}$ for land and ocean, respectively.[10] In this study, we find that the increased Hg^0 dry deposition to land and ocean Hg^0 evasion further partition the sink of primary Hg emissions to the land, consistent with Feinberg et al.[18] This implies that the regional anthropogenic emissions are more retained by local soil and vegetation, which probably causes a larger local impact but a smaller global impact than previously thought.[40,41] A recent study also found that an intact forest in the Peruvian Amazon intercepts large amounts of Hg emissions from nearby artisanal gold mining activities.[42] A similar intercept effect can be expected for East Asia, Southeast Asia, and Central Africa, where anthropogenic emissions are high but covered by tropical/subtropical forests (Figure S10). These updates thus need to be considered for a more accurate source-receptor relationship for the emissions from these regions, which is key for a successful effectiveness evaluation of the Minamata Convention on Mercury.

The simulated global total Hg emissions to the atmosphere amount to 12,000 Mg $year^{-1}$, with primary emissions of 2,590 Mg $year^{-1}$ (2,340 Mg $year^{-1}$ from anthropogenic sources and 250 Mg $year^{-1}$ from geogenic sources) and re-emissions of 2,000 Mg $year^{-1}$ and 7,200 Mg $year^{-1}$ from the land (including biomass burning) and ocean, respectively (Figure 1). This is 40% higher than in previous studies (8,500–8,700 Mg $year^{-1}$)[3,10,26] because of the potentially higher re-emissions from the ocean in this study. The modeled surface atmospheric Hg^0 concentrations and Hg^{II} wet deposition fluxes are still comparable with available observations (Figures S1 and S2), given a relatively large uncertainty range. Our model simulates an atmospheric Hg mass of 4,500 Mg with 3,800 Mg in the troposphere, consistent with observationally constrained ~4,000 Mg for tropospheric Hg mass.[43] The photo-reduction of Hg^{II}-organic complexes is 60% lower in our model, which results in stronger net oxidation to balance the higher total atmospheric emissions. This also results in a slightly shorter tropospheric Hg lifetime against deposition (3.8 months) than in Shah et al.[10] (5.5 months). However, there is still a lack of direct measurements of the atmospheric Hg redox rates and the model uncertainty for the abundance of important Hg^0 oxidants; e.g., Br/BrO is also as large as a factor of two.[26,44] Overall, our updated model is within the constraint of available observations (Figures S1–S5) and shows similar levels of agreement with observations compared with the reference models (Table S1). We simulate a likely stronger Hg^0 exchange and shorter turnover timescale between the atmosphere and land/ocean pools than previously recognized, reflecting our recent advance in understanding Hg processes and fluxes.

Fate of anthropogenic emissions

We find the land potentially as the largest sink of primary atmospheric emissions during 2005–2019 (Figure 2A), similar to the budget of 2012, as discussed above (Figure 1). The primary

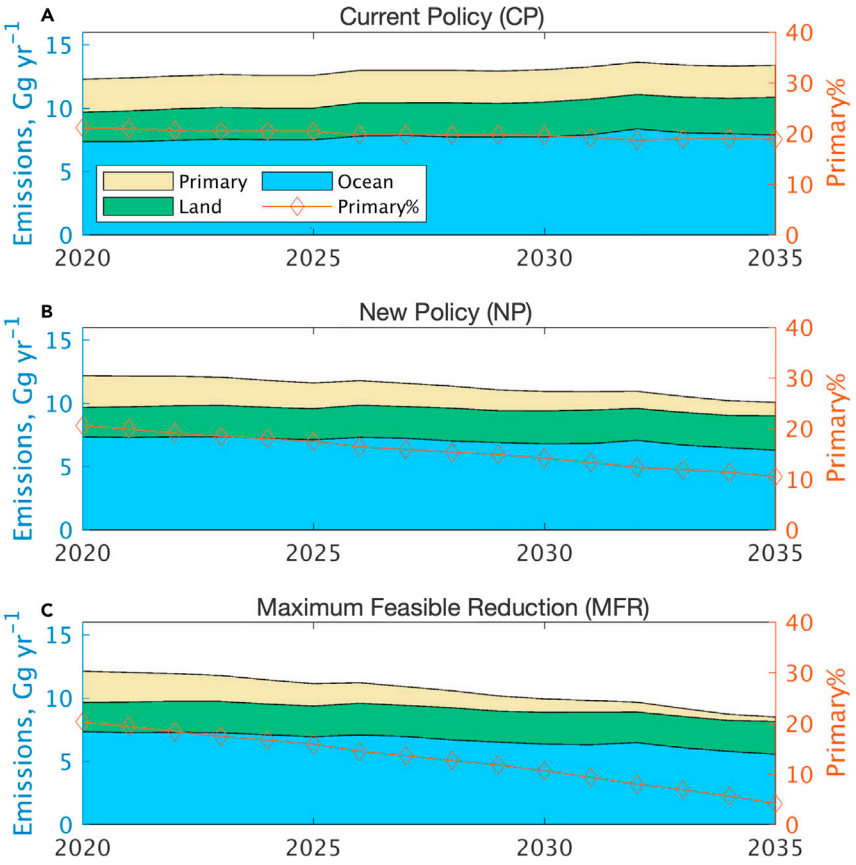

Figure 3. Projected primary versus re-emissions of Hg to the atmosphere during 2020–2035

(A) The CP scenario.

(B and C) The NP (B) and MFR (C) scenarios.

The orange lines are the fractions of primary anthropogenic over total atmospheric emissions.

anthropogenic emissions to the atmosphere increased from 1,964 Mg year^{-1} in 2000 to 2,390 Mg year^{-1} in 2015, with an average growth rate of 1.78% year^{-1} during 2010–2015.[17] The total cumulated primary emissions amount to 38,200 Mg during 2005–2019 and drove a slightly increased atmospheric Hg mass by 500 Mg during the 15 years, as suggested by our model (Figure 2A). The remaining 37,700 Mg emissions are predicted to be buried in land (25,900 Mg or 1,730 Mg year^{-1}, 68%) and ocean (12,300 Mg or 820 Mg year^{-1}, 32%).

The future anthropogenic emissions during 2020–2035 are also predicted to be mainly sequestered by the land environment (Figures 2B–2D). We consider three emission scenarios for 2035 following Pacyna et al.:[45] (1) current policy (CP), in which the emissions are almost steady as the Hg emission increase driven by a growing population/economy is offset by implementation of control measures and practices that are decided at present; (2) new policy (NP), in which the Hg emissions are substantially reduced as a co-benefit of reducing greenhouse gas emissions; and (3) maximum feasible reduction (MFR), in which all countries reach the highest feasible/available reduction efficiency in each emission sector. The CP, NP, and MFR scenarios project a global total anthropogenic emission of 1,960, 1,020, and 300 Mg year^{-1}, respectively, in 2035, and linearly routing the current emissions to this year results in cumulated anthropogenic emissions of 36,200, 28,100, and 21,900 Mg, respectively. Our model simulates a slightly increased (+200 Mg) atmospheric Hg mass for the CP scenario, while the NP and MFR scenarios result in a decrease of 1,000 Mg and 1,400 Mg, respectively. The fractions of the primary emissions (including anthropogenic and geogenic emissions) buried in the land during 2020–2035 are predicted to be close to 68% for all three scenarios (Figures 2B–2D), close to the value for 2005–2019 (Figure 2A).

Lower environmental sensitivities

The re-emissions of Hg from land and ocean may buffer the effect on environmental Hg levels by controlling the primary emissions in the future because the re-emissions are modeled to change much slower than the primary sources (Figure 3). The CP scenario simulates an increase of total atmospheric Hg emissions from 12,000 Mg year^{-1} in 2020 to 13,000 Mg year^{-1} in 2035, with the land and ocean re-emissions increasing from 2,300 to 7,300 Mg year^{-1} to 2,900 and 7,900 Mg year^{-1}, respectively. The fraction of primary anthropogenic emissions is predicted to keep steady (19%–21%) during this period. While the NP and MFR scenarios project primary anthropogenic emission decreases by 58% and 86% during 2020–2035, respectively, the re-emissions may only decrease by 17% and 25%, resulting in 25% and 37% decreases in total atmospheric emissions. The fractions of primary anthropogenic emissions over the total are predicted to be only 11% and 4.1% in 2035 for the NP and MFR scenarios, respectively (Figure 3).

The projected changes in atmospheric deposition reflect that of total atmospheric emissions at a decadal timescale given the proposed 3.8 months of lifetime for atmospheric Hg against deposition (Figures 4A and 4B). Compared with the level in 2020, the projected decrease in surface seawater methylmercury (MeHg) concentrations, which are more relevant to human exposure, is 9.5% and 17% for NP and MFR in 2035 (Figure 4C), respectively, smaller than the changes in atmospheric deposition (19% and 31%, respectively). It is largely caused by upwelling of subsurface waters enriched with inorganic Hg and MeHg.[7,15,24] The likely higher fraction of Hg^0 in the total atmospheric deposition to the ocean (40% versus 30% as previously estimated) also reduces the methylation efficiency because only Hg^{II} is ready to be methylated.[15] Overall, our study suggests that the marginal effect of abating anthropogenic Hg emissions diminishes with more thorough control, further dampening along the chain of processes from anthropogenic emissions to seawater MeHg concentrations and potential human exposure. Variability caused by climate and other environmental factors would be

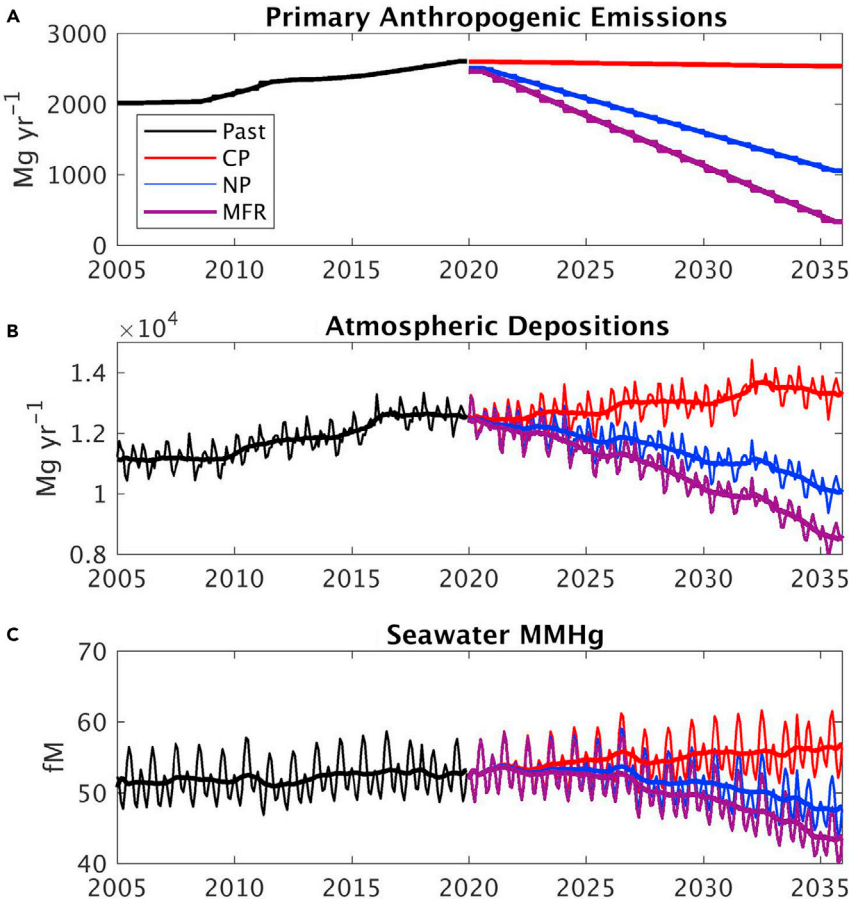

Figure 4. Modeled trends of environmental Hg levels during 2005–2035

(A) Primary anthropogenic emission to the atmosphere.

(B and C) Total atmospheric Hg deposition, including Hg^0, Hg^{II}, and Hg(P).

(C) Global average surface seawater (0–100 m) MeHg concentrations.

Three scenarios are considered during 2020–2035: CP, NP, and MFR, following Pacyna et al.[45] The bolded lines are yearly running means with the thinner lines as monthly values.

more pronounced and may offset the effects of anthropogenic emission reduction.[46]

Our updated global Hg budget proposes 40% higher total atmospheric emissions than previously estimated, which suggests a lower sensitivity of atmospheric levels to anthropogenic emissions. The legacy emissions sequestered in the terrestrial and marine environment may play a more important role than previously recognized. Although it is hard to directly compare with previous studies because of different model setups, we indeed predict smaller changes in atmospheric deposition responding to emission reductions. Taking two studies using the same future emission inventories as we do as an example, compared with a 19% and 31% decrease in 2035 for NP and MFR scenarios, respectively, in our study, Pacyna et al.[45] project a 20%–30% decrease for the NP scenario and 35%–50% in the northern hemisphere and 30–35% in the southern hemisphere for the MFR scenario; Angot et al.[47] also project a 24% decrease for the NP scenario compared with the CP one.

Uncertainties and implications

Our model results are subject to significant uncertainties from a few sources. One is from the GEOS-Chem model representation of atmospheric chemistry and physical processes, such as anthropogenic emissions, atmospheric transport, and redox chemistry, which can be represented by the normalized root-mean-square error between the modeled and observed ground-level total atmospheric Hg levels (30%). Our ability to develop a global atmospheric Hg budget is also limited by existing scientific knowledge and observations. Compared with a reference model developed by Shah et al.,[10] even though both models generally agree with existing data of Hg content in the atmosphere, ocean, and soils, we notice a multiplicity of solutions for the exchange fluxes between the atmosphere and the land/ocean. The variabilities among our model and previous modeling studies could represent the overall model uncertainties for the global Hg budget. For example, the ocean re-emissions and vegetation uptake of Hg^0 vary by approximately 30% and 50%, respectively. Further reducing the uncertainty requires more observations of these exchange fluxes. Large-scale Hg isotopic signatures also provide useful constraints for the relative magnitudes of many such fluxes.[13] The global Hg budget thus evolves with scientific advances and new data. Furthermore, the model simulates an increasing atmospheric abundance during 2005–2020 (Figure 4B), driven by increasing anthropogenic emissions (Figure 4A). This contradicts the decreasing atmospheric Hg levels observed in the northern hemisphere.[48] Reconciling such an apparent paradox indeed merits further studies, especially to disentangle the potential contributions from changing re-emissions from the land and ocean.

Our findings imply that potentially a more aggressive decrease in primary anthropogenic emissions is required to achieve the goal of reducing environmental Hg levels. The recently proposed

more ambitious carbon emission reduction plans by major carbon emission countries (e.g., net-zero targets by China, the United States, the European Union, and India) are on the right track (https://www.un.org/en/climatechange/net-zero-coalition), which will have a substantial co-benefit for Hg emission reductions.[45,48] Nevertheless, artisanal and small-scale gold production, the largest source of global atmospheric Hg emissions, is projected to have a relatively small reduction rate in the future even under the MFR scenario.[45] More stringent control and potentially more international intervention are indeed required for this source.[49]

Global environmental change strongly influences the exchange of atmospheric Hg with the land and ocean, which are both important sinks for anthropogenic Hg emissions. The climate-vegetation-human nexus can substantially alter the land Hg sinks regionally and globally (e.g., changed temperature and precipitation, decreased tropical forest area, and CO_2 fertilization), potentially increasing fire frequencies, and increased afforestation in the northern mid-latitudes.[21] Similarly, the increase in seawater temperature and acidity, weaker wind, enhanced light penetration, coastal eutrophication, and decreased productivity largely impact the ability of the ocean to absorb anthropogenic Hg emissions.[50] Although our model is not yet able to consider these factors, they need to be considered when evaluating the fate of future anthropogenic emissions, especially over a longer term, when climate change impact is more pronounced.

EXPERIMENTAL PROCEDURES

Resource availability

Lead contact

Further information and requests for resources and reagents should be directed to and will be fulfilled by the lead contact, Yanxu Zhang (zhangyx@nju.edu.cn).

Materials availability

This study did not generate new unique materials.

Data and code availability

The GEOS-Chem code and GTMM model code are available at https://www.geos-chem.seas.harvard.edu. The MITgcm model code is available on GitHub (https://github.com/MITgcm/MITgcm.git). Other code and datasets have been deposited at Mendeley Data (https://doi.org/10.17632/gbnnv93f7v.1). Any additional information required to reanalyze the data reported in this paper is available from the lead contact upon request.

General model description

The GEOS-Chem Hg model simulates the atmospheric redox chemistry, transport, and deposition of Hg species at a horizontal resolution of 4° latitude by 5° longitude and 47 vertical layers. The time step of the model is 10 min. The model is driven by MERRA2 re-analysis meteorological data. The Hg redox chemistry includes the initial oxidation of Hg^0 by Br and OH, subsequent oxidation of monovalent Hg (Hg^I) by ozone and radicals, and Hg^{II} photolysis in the gas and aqueous phases.[10] The model also simulates Hg(P) by inorganic and organic aerosols as well as its dynamic partition with gaseous Hg^{II}.[10] The model uses the anthropogenic Hg emission inventory developed by Streets et al.,[17] which is for 2005–2015 and has a global total Hg emission of 2,300 Mg $year^{-1}$ with 1,400 Mg $year^{-1}$ as Hg^0 and 900 Mg $year^{-1}$ as Hg^{II} (including Hg(P)) in 2012. The growth rates during 2010–2015 are extended to 2016–2019 to estimate the emissions during these years.

The GTMM includes a mechanistic simulation of soil and terrestrial ecosystem inorganic Hg storage and emissions following the CASA terrestrial biogeochemical cycle model. The model has a horizontal resolution of 1° × 1° with a monthly time step. It is run as a module of the GEOS-Chem model by taking atmospheric deposition as input. The deposited Hg is distributed among leaf, litter, and different soil carbon pools, and the re-emission of Hg from these pools is returned to the GEOS-Chem model.[5]

The MITgcm Hg model simulates the global ocean circulation on a lat-lon-cap grid that has a nominal horizontal resolution of approximately 1° × 1° with 50 vertical layers and higher resolution at the equator (~0.5° latitude) and the Arctic (~30 km) based on the ECCO v4 framework.[51] The Hg simulation includes Hg redox chemistry in the seawater, the partitioning onto particulate organic carbon (POC), the subsequent sinking to the ocean floor,[15] and the riverine Hg discharge to the ocean.[14] The model time step is an hour. The air-sea exchange of Hg (including atmospheric Hg^{II} deposition to the ocean and bidirectional exchange of Hg^0) is handled by the NJUCPL.[16]

GEOS-chem update

The dry deposition velocity of Hg^0 over land is calculated by a resistance in series approach.[52] We include the dry deposition velocity of Hg^0 by increasing its biological reactivity (f_0) following Feinberg et al.;[18] the f_0 of Hg^0 is increased from 1×10^{-5} to 3×10^{-5} globally following Hg vegetation uptake measurements,[19,53–56] and the f_0 value is increased to 0.2 over the rainforest to be consistent with micrometeorological flux tower data over the Amazon.[12] We further increase the f_0 value to 9×10^{-5} over tundra ecosystems to match a ratio of Hg^0:Hg^{II} deposition flux of 7:3 over this region.[11]

The loss of Hg^{II} to sea-salt aerosols in the marine boundary layer (MBL) is modeled as a first-order kinetic process limited by the mass transfer of Hg^{II} species to particles.[57] The loss rate is parameterized as a function of wind speed and humidity to match the observed gaseous Hg^{II} concentrations, which were measured with a KCl-coated denuder method. Later studies suggest that such a method may be significantly biased low because of the low Hg^{II} collection efficacy by the KCl denuder.[58] This is especially true over high-humidity conditions in the MBL. He and Mason[59] found, on average, an 80% lower bias for the KCl denuder method compared with cation exchange membrane methods over the tropical and north Pacific oceans. We therefore decrease the loss rate of Hg^{II} to sea-salt aerosol by 80% to compensate for the actually much higher gaseous Hg^{II} concentrations than used by Holmes et al.[57]

GTMM update

In the GTMM, approximately one-quarter of the Hg^0 and Hg^{II} dry deposition is partitioned to the interior leaf pools, with the remaining to the surface leaf/soil pool. In this study, we assume that all of the Hg^0 dry deposition is incorporated into the interior leaf pool, reflecting the high stomatal uptake of Hg^0 found by recent studies.[11,19] We assume that all of the Hg^{II} dry deposition is incorporated into the surface leaf/soil pool because there is no direct evidence to support the stomatal uptake of Hg^{II}.[20] The photoreduction of dry and wet deposited Hg^{II} in the surface soil/leaf pool is also decreased by a factor of 10 following Amos et al.[24] We also reduce the re-emission of Hg^0 from its associated soil organic carbon pool after decomposition by 50%, reflecting greater retention of Hg by the terrestrial environment.[19,25]

The Hg^0 emissions from biomass burning are considered in the GEOS-Chem model based on the Global Fire Emission Database (GFED v.4), and the monthly Hg^0 emission flux is calculated based on the carbon emissions and a Hg:CO ratio.[43] In this study, we double this ratio to reflect higher biomass burning Hg emissions suggested by recent studies such as Friedli et al.,[60] Kumar et al.,[61] and Shi et al.[62] The emitted Hg^0 from biomass burning is also subtracted from vegetation and land pools in the GTMM to achieve a mass balance. The subtraction starts from the surface leaf and soil pool but is extended to the fast, intermediate, slow, and armored organic soil pools, in that order, when the preceding Hg pool is exhausted.

MITgcm update

The sinking of seawater Hg^{II} that is bound to POC is the dominant pathway (also known as the biological pump) for anthropogenic Hg entering the deep ocean.[8] The modeled sinking flux of POC decreases exponentially with depth because of the continuous remineralization process by microbes on these sinking particles.[63] We find a significant underestimation of the Hg accumulation flux over the deep ocean, as suggested by Sanei et al.[64] and Liu et al.[37] This reflects the existence of a fast sinking and/or refractive sinking POC pool. In this study, we consider this pool following Kawai et al.[65] The magnitude of this fast or refractory sinking POC flux is assumed to be ~5% of the

total flux out of the euphotic layer and kept unchanged through the water column.

The air-sea exchange of Hg^0 is influenced by the concentration gradient across the interface and the piston velocity, which is modeled as a non-linear function of wind speed.[28] Different modeling schemes have been developed for the piston velocity calculation.[28–31,66] The influence of different schemes has been investigated by Zhang et al.;[16] however, it is not discernable by current observations of surface ocean Hg^0 concentrations and exchange fluxes. In this study, we use the McGillis et al.[31] scheme, which assumes a cubic function of wind speed and simulates the highest piston velocity among these schemes.

SUPPLEMENTAL INFORMATION

Supplemental information can be found online at https://doi.org/10.1016/j.oneear.2023.02.004.

ACKNOWLEDGMENTS

We thank Aryeh Feinberg and Anne L. Soerensen for helpful discussions and comments. Y.Z. acknowledges financial support from the National Natural Science Foundation of China (grant 42177349), the Fundamental Research Funds for Cornell University (14380168), and the Collaborative Innovation Center of Climate Change, Jiangsu Province. We acknowledge the researchers involved in collecting, analyzing, and sharing the atmosphere, river, and ocean Hg data included in our compilation dataset. We thank Jeroen E. Sonke and the other two anonymous reviewers for their helpful comments and suggestions.

AUTHOR CONTRIBUTIONS

Y.Z. designed and performed the study. P.Z., Z.S., S.H., T.Y., and P.W. conducted data analyses and visualization. V.S., M.L., J.Z., and Y.A. provided model code and/or observational datasets. Y.Z. wrote the original draft, with all other authors reviewing and editing.

DECLARATION OF INTERESTS

The authors declare no competing interests.

INCLUSION AND DIVERSITY

We support inclusive, diverse, and equitable conduct of research.

Received: June 20, 2022
Revised: December 1, 2022
Accepted: February 17, 2023
Published: March 17, 2023

REFERENCES

1. Zhang, Y., Song, Z., Huang, S., Zhang, P., Peng, Y., Wu, P., Gu, J., Dutkiewicz, S., Zhang, H., Wu, S., et al. (2021). Global health effects of future atmospheric mercury emissions. Nat. Commun. *12*, 3035. https://doi.org/10.1038/s41467-021-23391-7.
2. Selin, N.E. (2009). Global biogeochemical cycling of mercury: a review. Annu. Rev. Environ. Resour. *34*, 43–63. https://doi.org/10.1146/annurev.environ.051308.084314.
3. Outridge, P.M., Mason, R.P., Wang, F., Guerrero, S., and Heimbürger-Boavida, L.E. (2018). Updated global and oceanic mercury budgets for the united nations global mercury assessment 2018. Environ. Sci. Technol. *52*, 11466–11477. https://doi.org/10.1021/acs.est.8b01246.
4. Selin, N.E., Jacob, D.J., Yantosca, R.M., Strode, S., Jaeglé, L., and Sunderland, E.M. (2008). Global 3-D land-ocean-atmosphere model for mercury: present-day versus preindustrial cycles and anthropogenic enrichment factors for deposition. Global Biogeochem. Cycles *22*. https://doi.org/10.1029/2007GB003040.
5. Smith-Downey, N.V., Sunderland, E.M., and Jacob, D.J. (2010). Anthropogenic impacts on global storage and emissions of mercury from terrestrial soils: insights from a new global model. J. Geophys. Res. *115*, G03008. https://doi.org/10.1029/2009JG001124.
6. Soerensen, A.L., Sunderland, E.M., Holmes, C.D., Jacob, D.J., Yantosca, R.M., Skov, H., Christensen, J.H., Strode, S.A., and Mason, R.P. (2010). An improved global model for air-sea exchange of mercury: high concentrations over the North Atlantic. Environ. Sci. Technol. *44*, 8574–8580. https://doi.org/10.1021/es102032g.
7. Amos, H.M., Jacob, D.J., Streets, D.G., and Sunderland, E.M. (2013). Legacy impacts of all-time anthropogenic emissions on the global mercury cycle. Global Biogeochem. Cycles *27*, 410–421. https://doi.org/10.1002/gbc.20040.
8. Zhang, Y., Jaeglé, L., Thompson, L., and Streets, D.G. (2014). Six centuries of changing oceanic mercury. Global Biogeochem. Cycles *28*, 1251–1261. https://doi.org/10.1002/2014gb004939.
9. Saiz-Lopez, A., Travnikov, O., Sonke, J.E., Thackray, C.P., Jacob, D.J., Carmona-García, J., Francés-Monerris, A., Roca-Sanjuán, D., Acuña, A.U., Dávalos, J.Z., et al. (2020). Photochemistry of oxidized Hg(I) and Hg(II) species suggests missing mercury oxidation in the troposphere. Proc. Natl. Acad. Sci. USA *117*, 30949–30956. https://doi.org/10.1073/pnas.1922486117.
10. Shah, V., Jacob, D.J., Thackray, C.P., Wang, X., Sunderland, E.M., Dibble, T.S., Saiz-Lopez, A., Černušák, I., Kellö, V., Castro, P.J., et al. (2021). Improved mechanistic model of the atmospheric redox chemistry of mercury. Environ. Sci. Technol. *55*, 14445–14456. https://doi.org/10.1021/acs.est.1c03160.
11. Obrist, D., Agnan, Y., Jiskra, M., Olson, C.L., Colegrove, D.P., Hueber, J., Moore, C.W., Sonke, J.E., and Helmig, D. (2017). Tundra uptake of atmospheric elemental mercury drives Arctic mercury pollution. Nature *547*, 201–204. https://doi.org/10.1038/nature22997.
12. Fostier, A.H., Melendez-Perez, J.J., and Richter, L. (2015). Litter mercury deposition in the Amazonian rainforest. Environ. Pollut. *206*, 605–610. https://doi.org/10.1016/j.envpol.2015.08.010.
13. Jiskra, M., Heimbürger-Boavida, L.E., Desgranges, M.M., Petrova, M.V., Dufour, A., Ferreira-Araujo, B., Masbou, J., Chmeleff, J., Thyssen, M., Point, D., and Sonke, J.E. (2021). Mercury stable isotopes constrain atmospheric sources to the ocean. Nature *597*, 678–682. https://doi.org/10.1038/s41586-021-03859-8.
14. Liu, M., Zhang, Q., Maavara, T., Liu, S., Wang, X., and Raymond, P.A. (2021). Rivers as the largest source of mercury to coastal oceans worldwide. Nat. Geosci. *14*, 672–677. https://doi.org/10.1038/s41561-021-00793-2.
15. Zhang, Y., Soerensen, A.L., Schartup, A.T., and Sunderland, E.M. (2020). A global model for methylmercury formation and uptake at the base of marine food webs. Global Biogeochem. Cycles *34*. https://doi.org/10.1029/2019GB006348.
16. Zhang, Y., Horowitz, H., Wang, J., Xie, Z., Kuss, J., and Soerensen, A.L. (2019). A coupled global atmosphere-ocean model for air-sea exchange of mercury: insights into wet deposition and atmospheric redox chemistry. Environ. Sci. Technol. *53*, 5052–5061. https://doi.org/10.1021/acs.est.8b06205.
17. Streets, D.G., Horowitz, H.M., Lu, Z., Levin, L., Thackray, C.P., and Sunderland, E.M. (2019). Global and regional trends in mercury emissions and concentrations. Atmos. Environ. *201*, 2010–2015. https://doi.org/10.1016/j.atmosenv.2018.12.031.
18. Feinberg, A., Dlamini, T., Jiskra, M., Shah, V., and Selin, N.E. (2022). Evaluating atmospheric mercury (Hg) uptake by vegetation in a chemistry-transport model. Environ. Sci. Process. Impacts *24*, 1303–1318. https://doi.org/10.1039/d2em00032f.
19. Obrist, D., Roy, E.M., Harrison, J.L., Kwong, C.F., Munger, J.W., Moosmüller, H., Romero, C.D., Sun, S., Zhou, J., and Commane, R. (2021). Previously unaccounted atmospheric mercury deposition in a midlatitude deciduous forest. Proc. Natl. Acad. Sci. USA *118*, e2105477118. https://doi.org/10.1073/pnas.2105477118.

20. Zhou, J., Obrist, D., Dastoor, A., Jiskra, M., and Ryjkov, A. (2021). Vegetation uptake of mercury and impacts on global cycling. Nat. Rev. Earth Environ. *2*, 269–284. https://doi.org/10.1038/s43017-021-00146-y.

21. Wang, X., Yuan, W., Lin, C.J., Zhang, L., Zhang, H., and Feng, X. (2019). Climate and vegetation as primary drivers for global mercury storage in surface soil. Environ. Sci. Technol. *53*, 10665–10675. https://doi.org/10.1021/acs.est.9b02386.

22. Agnan, Y., Le Dantec, T., Moore, C.W., Edwards, G.C., and Obrist, D. (2016). New constraints on terrestrial surface-atmosphere fluxes of gaseous elemental mercury using a global Database. Environ. Sci. Technol. *50*, 507–524. https://doi.org/10.1021/acs.est.5b04013.

23. Schuster, P.F., Schaefer, K.M., Aiken, G.R., Antweiler, R.C., Dewild, J.F., Gryziec, J.D., Gusmeroli, A., Hugelius, G., Jafarov, E., Krabbenhoft, D.P., et al. (2018). Permafrost stores a globally significant amount of mercury. Geophys. Res. Lett. *45*, 1463–1471. https://doi.org/10.1002/2017gl075571.

24. Amos, H.M., Jacob, D.J., Kocman, D., Horowitz, H.M., Zhang, Y., Dutkiewicz, S., Horvat, M., Corbitt, E.S., Krabbenhoft, D.P., and Sunderland, E.M. (2014). Global biogeochemical implications of mercury discharges from rivers and sediment burial. Environ. Sci. Technol. *48*, 9514–9522. https://doi.org/10.1021/es502134t.

25. Obrist, D., Pokharel, A.K., and Moore, C. (2014). Vertical profile measurements of soil air suggest immobilization of gaseous elemental mercury in mineral soil. Environ. Sci. Technol. *48*, 2242–2252. https://doi.org/10.1021/es4048297.

26. Horowitz, H.M., Jacob, D.J., Zhang, Y., Dibble, T.S., Slemr, F., Amos, H.M., Schmidt, J.A., Corbitt, E.S., Marais, E.A., and Sunderland, E.M. (2017). A new mechanism for atmospheric mercury redox chemistry: implications for the global mercury budget. Atmos. Chem. Phys. *17*, 6353–6371. https://doi.org/10.5194/acp-17-6353-2017.

27. Osterwalder, S., Nerentorp, M., Zhu, W., Jiskra, M., Nilsson, E., Nilsson, M.B., Rutgersson, A., Soerensen, A.L., Sommar, J., Wallin, M.B., et al. (2021). Critical observations of gaseous elemental mercury air-sea exchange. Global Biogeochem. Cycles *35*. https://doi.org/10.1029/2020GB006742.

28. Nightingale, P.D., Malin, G., Law, C.S., Watson, A.J., Liss, P.S., Liddicoat, M.I., Boutin, J., and Upstill-Goddard, R.C. (2000). In situ evaluation of air-sea gas exchange parameterizations using novel conservative and volatile tracers. Global Biogeochem. Cycles *14*, 373–387. https://doi.org/10.1029/1999gb900091.

29. Liss, P.S., and Merlivat, L. (1986). Air-sea gas exchange rates: introduction and synthesis. In The role of air-sea exchange in geochemical cycling (Springer), pp. 113–127. https://doi.org/10.1007/978-94-009-4738-2_5.

30. Wanninkhof, R., and McGillis, W.R. (1999). A cubic relationship between air-sea CO2 exchange and wind speed. Geophys. Res. Lett. *26*, 1889–1892. https://doi.org/10.1029/1999gl900363.

31. McGillis, W.R., Edson, J.B., Hare, J.E., and Fairall, C.W. (2001). Direct covariance air-sea CO2 fluxes. J. Geophys. Res. *106*, 16729–16745. https://doi.org/10.1029/2000jc000506.

32. Wanninkhof, R. (2014). Relationship between wind speed and gas exchange over the ocean revisited. Limnol Oceanogr. Methods *12*, 351–362. https://doi.org/10.4319/lom.2014.12.351.

33. Andersson, A., Rutgersson, A., and Sahlée, E. (2016). Using eddy covariance to estimate air-sea gas transfer velocity for oxygen. J. Mar. Syst. *159*, 67–75. https://doi.org/10.1016/j.jmarsys.2016.02.008.

34. Garbe, C.S., Rutgersson, A., Boutin, J., de Leeuw, G., Delille, B., Fairall, C.W., Gruber, N., Hare, J., Ho, D.T., Johnson, M.T., et al. (2014). Transfer across the air-sea interface. In Ocean-Atmosphere Interactions of Gases and Particles, pp. 55–112. https://doi.org/10.1007/978-3-642-25643-1_2.

35. Amos, H.M., Jacob, D.J., Holmes, C.D., Fisher, J.A., Wang, Q., Yantosca, R.M., Corbitt, E.S., Galarneau, E., Rutter, A.P., Gustin, M.S., et al. (2012). Gas-particle partitioning of atmospheric Hg(II) and its effect on global mercury deposition. Atmos. Chem. Phys. *12*, 591–603. https://doi.org/10.5194/acp-12-591-2012.

36. Zhang, Y., Jacob, D.J., Dutkiewicz, S., Amos, H.M., Long, M.S., and Sunderland, E.M. (2015). Biogeochemical drivers of the fate of riverine mercury discharged to the global and Arctic oceans. Global Biogeochem. Cycles *29*, 854–864. https://doi.org/10.1002/2015gb005124.

37. Liu, M., Xiao, W., Zhang, Q., Yuan, S., Raymond, P.A., Chen, J., Liu, J., Tao, S., Xu, Y., and Wang, X. (2021). Substantial accumulation of mercury in the deepest parts of the ocean and implications for the environmental mercury cycle. Proc. Natl. Acad. Sci. USA *118*, e2102629118. https://doi.org/10.1073/pnas.2102629118.

38. Sunderland, E.M. (2007). Mercury exposure from domestic and imported estuarine and marine fish in the US seafood market. Environ. Health Perspect. *115*, 235–242. https://doi.org/10.1289/ehp.9377.

39. Sonke, J.E., Teisserenc, R., Heimbürger-Boavida, L.E., Petrova, M.V., Marusczak, N., Le Dantec, T., Chupakov, A.V., Li, C., Thackray, C.P., Sunderland, E.M., et al. (2018). Eurasian river spring flood observations support net Arctic Ocean mercury export to the atmosphere and Atlantic Ocean. Proc. Natl. Acad. Sci. USA *115*, E11586–E11594. https://doi.org/10.1073/pnas.1811957115.

40. Corbitt, E.S., Jacob, D.J., Holmes, C.D., Streets, D.G., and Sunderland, E.M. (2011). Global source-receptor relationships for mercury deposition under present-day and 2050 emissions scenarios. Environ. Sci. Technol. *45*, 10477–10484. https://doi.org/10.1021/es202496y.

41. Chen, L., Zhang, W., Zhang, Y., Tong, Y., Liu, M., Wang, H., Xie, H., and Wang, X. (2018). Historical and future trends in global source-receptor relationships of mercury. Sci. Total Environ. *610*, 24–31. https://doi.org/10.1016/j.scitotenv.2017.07.182.

42. Gerson, J.R., Szponar, N., Zambrano, A.A., Bergquist, B., Broadbent, E., Driscoll, C.T., Erkenswick, G., Evers, D.C., Fernandez, L.E., Hsu-Kim, H., et al. (2022). Amazon forests capture high levels of atmospheric mercury pollution from artisanal gold mining. Nat. Commun. *13*, 559. https://doi.org/10.1038/s41467-022-27997-3.

43. Holmes, C.D., Jacob, D.J., Corbitt, E.S., Mao, J., Yang, X., Talbot, R., and Slemr, F. (2010). Global atmospheric model for mercury including oxidation by bromine atoms. Atmos. Chem. Phys. *10*, 12037–12057. https://doi.org/10.5194/acp-10-12037-2010.

44. Wang, X., Jacob, D.J., Downs, W., Zhai, S., Zhu, L., Shah, V., Holmes, C.D., Sherwen, T., Alexander, B., Evans, M.J., et al. (2021). Global tropospheric halogen (Cl, Br, I) chemistry and its impact on oxidants. Atmos. Chem. Phys. *21*, 13973–13996. https://doi.org/10.5194/acp-21-13973-2021.

45. Pacyna, J.M., Travnikov, O., De Simone, F., Hedgecock, I.M., Sundseth, K., Pacyna, E.G., Steenhuisen, F., Pirrone, N., Munthe, J., and Kindbom, K. (2016). Current and future levels of mercury atmospheric pollution on a global scale. Atmos. Chem. Phys. *16*, 12495–12511. https://doi.org/10.5194/acp-16-12495-2016.

46. Wang, F., Outridge, P.M., Feng, X., Meng, B., Heimbürger-Boavida, L.E., and Mason, R.P. (2019). How closely do mercury trends in fish and other aquatic wildlife track those in the atmosphere?–Implications for evaluating the effectiveness of the Minamata Convention. Sci. Total Environ. *674*, 58–70.

47. Angot, H., Hoffman, N., Giang, A., Thackray, C.P., Hendricks, A.N., Urban, N.R., and Selin, N.E. (2018). Global and local impacts of delayed mercury mitigation efforts. Environ. Sci. Technol. *52*, 12968–12977. https://doi.org/10.1021/acs.est.8b04542.

48. Zhang, Y., Jacob, D.J., Horowitz, H.M., Chen, L., Amos, H.M., Krabbenhoft, D.P., Slemr, F., St Louis, V.L., and Sunderland, E.M. (2016). Observed decrease in atmospheric mercury explained by global decline in anthropogenic emissions. Proc. Natl. Acad. Sci. USA *113*, 526–531. https://doi.org/10.1073/pnas.1516312113.

49. Pang, Q., Gu, J., Wang, H., and Zhang, Y. (2022). Global health impact of atmospheric mercury emissions from artisanal and small-scale gold mining. iScience *25*, 104881. https://doi.org/10.1016/j.isci.2022.104881.

50. Zhang, Y., Dutkiewicz, S., and Sunderland, E.M. (2021). Impacts of climate change on methylmercury formation and bioaccumulation in the 21st century ocean. One Earth *4*, 279–288. https://doi.org/10.1016/j.oneear.2021.01.005.

51. Forget, G., Campin, J.M., Heimbach, P., Hill, C.N., Ponte, R.M., and Wunsch, C. (2015). ECCO version 4: an integrated framework for non-linear inverse modeling and global ocean state estimation. Geosci. Model Dev. (GMD) *8*, 3071–3104. https://doi.org/10.5194/gmd-8-3071-2015.

52. Wesely, M.L., and Lesht, B.M. (1989). Comparison of radm dry deposition algorithms with a site-specific method for inferring dry deposition. Water Air Soil Pollut. *44*, 273–293. https://doi.org/10.1007/Bf00279259.

53. Demers, J.D., Blum, J.D., and Zak, D.R. (2013). Mercury isotopes in a forested ecosystem: implications for air-surface exchange dynamics and the global mercury cycle. Global Biogeochem. Cycles *27*, 222–238. https://doi.org/10.1002/gbc.20021.

54. Jiskra, M., Wiederhold, J.G., Skyllberg, U., Kronberg, R.M., Hajdas, I., and Kretzschmar, R. (2015). Mercury deposition and re-emission pathways in boreal forest soils investigated with Hg isotope signatures. Environ. Sci. Technol. *49*, 7188–7196. https://doi.org/10.1021/acs.est.5b00742.

55. Zheng, W., Obrist, D., Weis, D., and Bergquist, B.A. (2016). Mercury isotope compositions across North American forests. Global Biogeochem. Cycles *30*, 1475–1492. https://doi.org/10.1002/2015gb005323.

56. Wang, X., Bao, Z., Lin, C.J., Yuan, W., and Feng, X. (2016). Assessment of global mercury deposition through litterfall. Environ. Sci. Technol. *50*, 8548–8557. https://doi.org/10.1021/acs.est.5b06351.

57. Holmes, C.D., Jacob, D.J., Mason, R.P., and Jaffe, D.A. (2009). Sources and deposition of reactive gaseous mercury in the marine atmosphere. Atmos. Environ. *43*, 2278–2285. https://doi.org/10.1016/j.atmosenv.2009.01.051.

58. Lyman, S.N., and Gustin, M.S. (2009). Determinants of atmospheric mercury concentrations in Reno, Nevada. Sci. Total Environ. *408*, 431–438. https://doi.org/10.1016/j.scitotenv.2009.09.045.

59. He, Y., and Mason, R.P. (2021). Comparison of reactive gaseous mercury measured by KCl-coated denuders and cation exchange membranes during the Pacific GEOTRACES GP15 expedition. Atmos. Environ. *244*, 117973. https://doi.org/10.1016/j.atmosenv.2020.117973.

60. Friedli, H.R., Arellano, A.F., Cinnirella, S., and Pirrone, N. (2009). Mercury emissions from global biomass burning: spatialand temporal distribution. In Mercury fate and transport in the global atmosphere (Springer), pp. 193–220. https://doi.org/10.1007/978-0-387-93958-2_8.

61. Kumar, A., Wu, S., Huang, Y., Liao, H., and Kaplan, J.O. (2018). Mercury from wildfires: global emission inventories and sensitivity to 2000-2050 global change. Atmos. Environ. *173*, 6–15. https://doi.org/10.1016/j.atmosenv.2017.10.061.

62. Shi, Y., Zhao, A., Matsunaga, T., Yamaguchi, Y., Zang, S., Li, Z., Yu, T., and Gu, X. (2019). High-resolution inventory of mercury emissions from biomass burning in tropical continents during 2001-2017. Sci. Total Environ. *653*, 638–648. https://doi.org/10.1016/j.scitotenv.2018.10.420.

63. Dutkiewicz, S., Follows, M.J., and Bragg, J.G. (2009). Modeling the coupling of ocean ecology and biogeochemistry. Global Biogeochem. Cycles *23*. https://doi.org/10.1029/2008gb003405.

64. Sanei, H., Outridge, P.M., Oguri, K., Stern, G.A., Thamdrup, B., Wenzhöfer, F., Wang, F., and Glud, R.N. (2021). High mercury accumulation in deep-ocean hadal sediments. Sci. Rep. *11*, 10970. https://doi.org/10.1038/s41598-021-90459-1.

65. Kawai, T., Sakurai, T., and Suzuki, N. (2020). Application of a new dynamic 3-D model to investigate human impacts on the fate of mercury in the global ocean. Environ. Model. Software *124*, 104599. https://doi.org/10.1016/j.envsoft.2019.104599.

66. Wanninkhof, R. (1992). Relationship between wind-speed and gas-exchange over the ocean. J. Geophys. Res. *97*, 7373–7382. https://doi.org/10.1029/92jc00188.